Submitted to the Astrophysical Journal Letters, 11 Feb 2002; accepted 19 March 2002.
Preprint typeset using LaTeX style emulateapj v. 11/12/01

THE DISCOVERY OF TIME VARIABILITY IN OH MEGAMASERS

Jeremy Darling & Riccardo Giovanelli
Department of Astronomy and National Astronomy and Ionosphere Center, Cornell University, 524 Space Sciences Building, Ithaca, NY 14853; darling@astro.cornell.edu; riccardo@astro.cornell.edu
Submitted to the Astrophysical Journal Letters, 11 Feb 2002; accepted 19 March 2002.

ABSTRACT

We report the discovery of variability in the OH megamaser in IRAS 21272+2514 at $z = 0.15$. This is the first OH megamaser (OHM) observed to vary in time. The variation is broadband, spanning 0.5–1.5 MHz or 100–300 km s^{-1} in the rest frame, and strong, showing *rms* modulations of 10%–15% while the largest change in flux density between extremal epochs is 34%. Timescales sampled range from 39 to 821 days, and the characteristic modulation timescale is likely to be less than the shortest time baseline. The source of modulation is currently ambiguous, although we favor interstellar scintillation. Best estimates of the size scales of the 1667 MHz OH line features obtained from refractive interstellar scintillation models constrain variable features to be smaller than 2 pc, and quiescent features to be larger than a few pc. Compact masers account for roughly 27%–58% of the total OH emission in this source. Accelerations in spectral lines are generally constrained to be less than 3 km s^{-1} yr^{-1}, but acceleration of this magnitude is suggested in one of the quiescent spectral components and merits further study.

Subject headings: galaxies: individual (IRAS 21272+2514) — galaxies: starburst — masers — radio lines: galaxies — scattering

1. INTRODUCTION

The OH megamaser (OHM) in IRAS 21272+2514 was discovered in August 1999 and reobserved in October 1999 as part of the Arecibo[1] OHM survey (Darling & Giovanelli 2000, 2001, 2002a). Spectra of this strong megamaser spanning 85 days showed a remarkable change in some, but not all, spectral features. This is the first documented detection of variability in an OHM, and it suggests that many OHMs may exhibit variability on time scales of days to months. Observations of variability can segregate maser emission into compact (variable) and extended (quiescent) emission in a similar and complementary manner to very long baseline interferometry (VLBI) observations which show that roughly two-thirds of OHM emission is compact (Lonsdale *et al.* 1998; Diamond *et al.* 1999; Pihlström *et al.* 2001).

IRAS 21272+2514 has a heliocentric optical redshift $z = 0.15102 \pm 0.00012$, while the bulk of the multi-component OH emission is blueshifted with respect to the optical, spanning 849 km s^{-1} in the rest frame at 10% of peak flux density and centered on $z_{OH} = 0.15021 \pm 0.00005$ (Darling & Giovanelli 2000, 2002b). The integrated OH luminosity is among the highest known at $L_{OH} = 4.57 \times 10^3 L_\odot$,[2] and the far-IR (FIR) luminosity is constrained to be in the range $L_{FIR} = (4.9\text{–}7.8) \times 10^{11} L_\odot$ (the 100 μm flux is undetected by IRAS). The 1.4 GHz flux density is modest, at 4.4 ± 0.5 mJy (Condon *et al.* 1998), and IRAS 21272+2514 has some IR excess but is broadly consistent with the radio-FIR relationship for star forming galaxies (Darling & Giovanelli 2002a). This object has a Seyfert 2 nucleus (Darling & Giovanelli 2002b).

In this letter, we present follow-up observations of IRAS 21272+2514 designed to confirm the observed variability (§2), we discuss the modulation present in the OH spectral line components (§3), we set limits on the size scales of all observed maser components (§4), we constrain accelerations in the OH spectral lines (§5), and we discuss the implications of variability for understanding OHMs and the environments which produce them (§6).

[1] The Arecibo Observatory is part of the National Astronomy and Ionosphere Center, which is operated by Cornell University under a cooperative agreement with the National Science Foundation.

[2] We assume $H_\circ = 75$ km s^{-1} Mpc^{-1}, $\Omega_M = 0.3$, and $\Omega_\Lambda = 0.7$.

2. OBSERVATIONS AND DATA REDUCTION

Observations were performed at Arecibo with the L-narrow and L-wide receivers as indicated in Table 1, nodding on- and off-source for 4 minutes each. We record spectra in 1-sec intervals in two circular polarizations to facilitate radio frequency interference (RFI) excision as described in Darling & Giovanelli (2001). A weights spectrum is produced for each epoch which shows the fraction of RFI-free records used to construct each channel in a spectrum. The weights spectrum spanning all epochs used to construct the average spectrum shown in Figure 1 indicates that while some RFI is present in 1%–4% of the records, it is not the source of the observed spectral variation. Final spectra are averages of two circular polarizations which do not significantly differ except in channels with significant RFI.

Observations have been consolidated into five epochs to enhance the spectral signal to noise as indicated in Table 1. Effective modified Julian dates (MJD) are time-weighted averages of observing sessions within each epoch. Although the separation of observations within epochs spans 1–8 days, no variability is observed within epochs. Note that intraepoch variability is poorly constrained due to low signal-to-noise ratio.

Figure 1 shows the residual spectra (each epoch minus the average spectrum) from the five consolidated epochs, the average spectrum over all time, and the weights spectrum of the average. The main emission components are labeled in the average spectrum. The *rms* noise is 0.17 mJy in the average spectrum and typically 0.35 mJy in the residuals. The residual spectra show significant modulation only in emission line components 1 and 2. Spectra have been scaled to account for broadband changes in sensitivity and calibration as described in §3.

TABLE 1
JOURNAL OF OBSERVATIONS AND EPOCH CONSOLIDATION SCHEME

Date (UT)	Center UT (hr)	Receiver[a]	t_{on} (minutes)	MJD	Effective MJD	t_{tot} (minutes)
10 Aug 1999	04.60	L-wide	20	51400.1917		
18 Aug 1999	04.83	L-wide	12	51408.2012	51403.1953	32
25 Oct 1999	23.53	L-wide	4	51477.9804		
03 Nov 1999	22.39	L-wide	28	51485.9329	51484.9388	32
29 Sep 2000	01.10	L-narrow	12	51816.0458		
05 Oct 2000	00.56	L-narrow	12	51822.0233	51819.0345	24
02 Oct 2001	01.33	L-narrow	16	52184.0554		
03 Oct 2001	01.33	L-narrow	16	52185.0554	52184.5554	32
09 Nov 2001	23.34	L-narrow	8	52222.9725		
10 Nov 2001	23.29	L-narrow	12	52223.9671		
12 Nov 2001	23.18	L-narrow	8	52225.9658	52224.2540	28

[a]There are two L-band receivers in the Gregorian system at Arecibo: the L-wide receiver (1.12–1.73 GHz), and the L-narrow receiver (1.28–1.50 GHz).

3. SPECTRAL LINE MODULATION

Comparing measurements from different observing epochs can potentially introduce significant spurious time-dependent signals. The observations presented here bracket significant changes in the performance of the telescope, including a gross and fine refiguring of the primary surface, implementation of active control of the pointing with tie-downs anchoring the platform, refined pointing models, and general fine-tuning of the system. Observations were also performed with two different feeds (see Table 1). The solution to the significant changes between observing epochs lies in accurate calibration of the gain for each observing session, in the broadband nature of the changes in telescope performance, and in the complicated, multi-component spectrum of IRAS 21272+2514. Measuring *relative* changes between spectral features or changes of a given line as a fraction of the whole spectrum can resolve broadband calibration issues. Sources of spurious narrow-band variability (RFI) have been identified by their short timescales and excised.

Measurements of relative variations between spectral features or with respect to the total OH spectrum is complicated by the possibility that all spectral features may vary, and that the variable components make up a significant fraction of the total OH flux. We approach this problem iteratively, first identifying both the variable and the apparently quiescent features, then comparing the fluxes of quiescent features to the total quiescent flux over time to constrain the modulation actually present in each feature. Once stable spectral features have been identified, the variable features are measured with respect to the total quiescent flux to eliminate broadband instrumental variability between epochs.

Figure 2 shows for each spectral component labeled in Figure 1 the integrated flux density, the peak flux density, and the residual change in both scaled by the integrated spectrum minus spectral components 1 and 2. The average peak and integrated flux density of each spectral component is listed in columns (2) and (3) of Table 2. We find that components 1 and 2 show significant modulation of $10.4\% \pm 1.6\%$ and $14.4\% \pm 1.6\%$, respectively, while the remaining components do not show significant modulation (col. [4] of Table 2). The source modulation index m_s is the *rms* fluctuation of the integrated line flux density.

A useful diagnostic of the temporal structure of variability is the structure function: $D(\tau) = \langle [F(t) - F(t+\tau)]^2 \rangle_t$. The structure functions of lines 3 and 4 are consistent with zero for all 10 time baselines, whereas lines 1 and 2 show large and highly variable values which indicate characteristic timescales less than the shortest sampling interval of 39 days.

4. MASER SIZE SCALES

If the observed modulation is intrinsic to the source, then the usual light travel time constraint applies to the amplified continuum source rather than the masing gas if the masing is unsaturated (unless the variability is due to motions in the gas itself). Variation is observed on the shortest time baseline of 39 days, indicating that the variable source is no larger than 0.03 pc or 6.7 μac. If the masing region is of roughly the same size, it would have a brightness temperature of $T \approx 6 \times 10^{13}$ K. Such a small source would certainly scintillate. Hence, the observed variability is at least partly due to interstellar scintillation (ISS), and we choose the weaker constraint on the angular sizes of the variable masing regions by adopting ISS to interpret the observations.

Walker (1998) provides rough predictions of the scintillation properties of extragalactic sources based on the interstellar medium model of Taylor & Cordes (1993) which we apply to the observed variation in the OH line components of IRAS 21272+2514. The OH line radiation must pass through two scintillating screens, but the dominant influence will be from the electron screen in our own galaxy. The galactic coordinates of 21272+2514, $(l, b) = (75.7°, -18.4°)$, indicate a transition frequency from strong to weak scattering at $\nu_\circ = 15 \pm 1$ GHz and a first Fresnel zone at $\nu_\circ$ of size $\theta_{F\circ} = 2$ μas. At $\nu = 1.45$ GHz, the scattering should be strong refractive ISS (RISS). For a point source, Walker (1998) predicts a modulation index of $m_p = 27\%$, a scattering disk 0.34 mas in size, and a scintillation timescale of 10 days. We scale the point source modulation index m_p to match the observed modulation m_s in each source component to obtain rough estimates of source sizes and scintillation timescales from the scaling relations $\theta_s/\theta_p = (m_p/m_s)^{6/7}$ and $\tau_s/\tau_p = \theta_s/\theta_p$. Estimates of the angular sizes, RISS timescales, and physical sizes of the OH line components are listed in columns

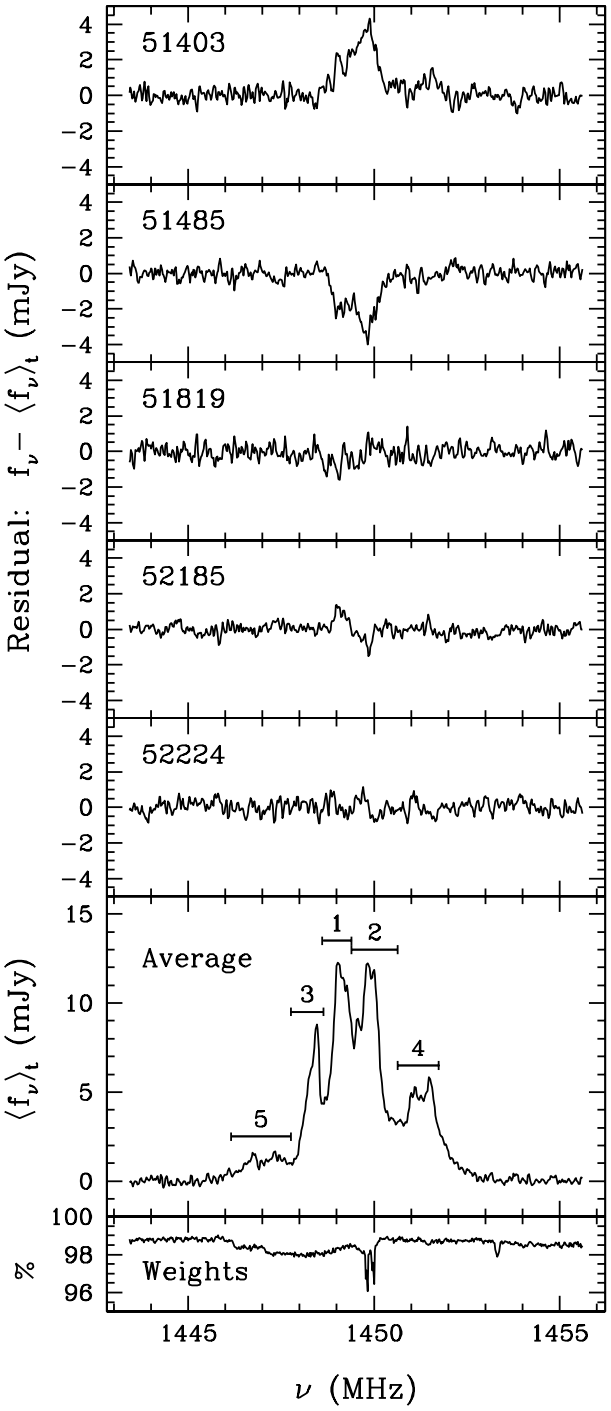

FIG. 1.— Residual spectra of IRAS 21272+2514 in the five consolidated epochs, each labeled by the MJD (Table 1), and the average spectrum with emission line components labeled. The spectra bracket an 821 day interval. The residuals show strong variability in this source, but only in components 1 and 2 of the emission line spectrum. Spectra have been scaled to account for broadband changes in sensitivity and calibration as described in §3. The weights spectrum indicates the percentage of data records used to construct each channel in the average spectrum and indicates channels where RFI was flagged and removed.

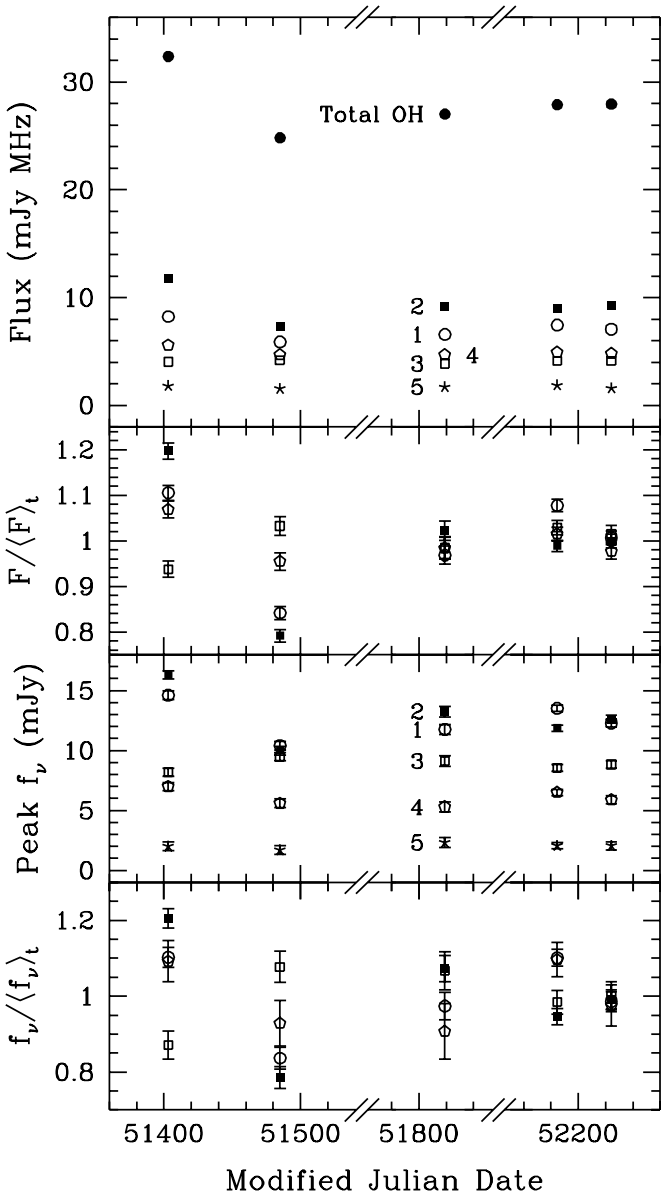

FIG. 2.— Integrated line flux and peak flux density measurements of the OH emission line components by epoch. Components are identified in Figure 1. The abscissa has been shortened to facilitate comparison of epochs. Component 5, which has low signal to noise and large error bars, is not shown in the residual plots.

(5)–(7) of Table 2. The two components which show strong modulation have submilliarcsecond angular sizes, are less than 2 pc in size, and are expected to show a characteristic RISS timescale of 17–22 days. This is in good agreement with the observations and our inability to observe changes on short time baselines of 1–8 days. This treatment assumes that all of the emission within a variable spectral component originates from the same compact region. It is also possible that part of the emission is compact and part is extended, so the scintillation predictions are actually upper limits on the source size and the RISS timescales may be as low as 10 days. If the compact variable features are smaller than the scattering disk, then they are expected to show the full point source modulation of 27% and must account for at least 39% and 53% of the emission seen in components 1 and 2, respectively. In other words, no more than roughly half of the emission in components 1 and 2 can be extended. These constraints on the fraction of compact emission present in OHMs are consistent with VLBI observations of nearby OHMs by Diamond *et al.* (1999) and others who find that roughly two-thirds of the total

OH emission is compact.

Components 3–5, which do not show significant modulation, are constrained to be larger than 1 mas or a few parsecs. RISS timescales in these components are constrained by their modulation indices to be larger than 28–51 days. Note that although observations span longer time baselines, the observed limits on modulation provide the stronger constraint — modulation may be present in components 3–5 on timescales of a few months, but the observations lack the sensitivity to detect variations of less than about 4%. The fraction of compact emission in components 3, 4, and 5 is less than 15%, 16%, and 30%, respectively.

5. ACCELERATION

Like water masers associated with AGN, one might expect OH megamasers to exhibit accelerations in emission line features. The kinematical structure of major mergers is certainly complicated and dynamic, and it is possible that accelerating masing gas will be observable over the timescales of this study. Water maser features in the best-studied case, NGC 4258, show accelerations of 9.3 km s^{-1} yr^{-1} along the line of sight (Herrnstein *et al.* 1999). Accelerations of this magnitude in OHM line features can be detected by this study if they exist. One might expect that since OHM emission profiles are thought to be an ensemble of many masing regions, then accelerations will be averaged out by the summation. This is especially true if OHMs are produced in highly turbulent or chaotic accumulations of molecular gas. The wide range of line profiles suggests that this may be the case, although there are a number of narrow, physically compact emission lines in the sample. It might be surprising if the lines showing intensity fluctuations do not show significant accelerations.

Overall, frequency/velocity residuals are consistent with the uncertainties in the line peaks of ±1 channel, corresponding to 24 kHz in the observer frame. The mean frequency of the peak of each spectral component is listed in column (8) of Table 2. The associated uncertainties are generally consistent with $\pm 24/\sqrt{N}$ kHz where N is the number of epochs used in the mean (N is listed in parentheses at the end of col. [9] of Table 2). Acceleration can be measured from the slope of a linear fit to the time series of line peak frequencies and expressed in the rest frame of the source by including a factor $(1+z)^2$ to account for time dilation and the narrowing of frequency intervals with redshift. The minimum detectable acceleration observable in an OHM line feature is set by the uncertainty of the best-fit slope obtained from N observations with velocity resolution ±4.4 km s^{-1}(observer frame):

$$\sigma_a = \frac{\sigma_v(1+z)}{\sigma_t\sqrt{N-1}} = (4.4 \text{ km s}^{-1} \text{ yr}^{-1})\frac{(1+z)^2}{\sigma_t(\text{yr})\sqrt{N-1}} \quad (1)$$

where σ_t^2 is the variance of the sampling in time and σ_v is the uncertainty of ±1 channel in identifying the peak of a line. For 21272+2514, with five epochs sampled, $\sigma_a = 2.8$ km s^{-1} yr^{-1}. This sets a rough lower limit on the line accelerations which may be measured from the available data.

Table 2 lists the rest frame line accelerations for each component from fits to the time series of line peaks. Uncertainties are obtained from the fits and N is listed in parentheses. Except component 2 where the peak could not be identified in one epoch, accelerations are obtained from fits to all data points. Line accelerations are consistent with zero except for line 3 which shows a 3.3 σ deviation from zero. The acceleration of -2.6 ± 0.8 km s^{-1} yr^{-1} for component 3 is very close to the expected lower detection limit of 2.8 km s^{-1} yr^{-1}. Confirmation of this acceleration requires re-observation, which will provide a longer time baseline. It is worth mention that the peaks of line 3 show a steady decrease in frequency over time with little scatter and no outliers. It is interesting that this line also shows no significant modulation in amplitude.

6. CONCLUSIONS

This brief study of IRAS 21272+2514 demonstrates the powerful constraints that variability studies can place on the emission regions of OHMs, including the segregation of different spectral components into different physical size scales. Better sampling of intermediate time scales can provide even stronger constraints on the source properties including the physical environments responsible for OHMs. There is mounting evidence that OHMs are composed of both diffuse and compact emission regions with different saturation states (Lonsdale *et al.* 1998; Diamond *et al.* 1999). This study obtains constraints on both the size and proportion of compact emission regions: compact features must be smaller than about 2 pc and account for 27%–58% of the total OH emission. To account for such high surface brightness emission we suggest that either shocks are involved in the pumping of OH or that these compact regions represent fortuitous geometries which provide enhanced masing path lengths as suggested by Pihlström *et al.* (2001). Accelerations of the OH lines of IRAS 21272+2514 are generally constrained to be less than 3 km s^{-1} yr^{-1}, although further observations are required to resolve suggestions of acceleration in one component.

Many thanks indeed to B. Catinella for obtaining the spectra of IRAS 21272+2514 during the MJD 52185 and 52224 epochs and to M. Walker for supplemental scintillation calculations. It is a pleasure to thank the staff of the Arecibo Observatory for excellent support. This work has received support from STScI grant 8373 and NSF grant AST 00-98526.

REFERENCES

Condon, J. J., Cotton, W. D., Greisen, E. W., Yin, Q. F., Perley, R. A., Taylor, G. B., & Broderick, J. J. 1998, AJ, 115, 1693
Darling, J. & Giovanelli, R. 2000, AJ, 119, 3003
Darling, J. & Giovanelli, R. 2001, AJ, 121, 1278
Darling, J. & Giovanelli, R. 2002a, AJ, submitted
Darling, J. & Giovanelli, R. 2002b, AJ, in preparation
Diamond, P. J., Lonsdale, C. J., Lonsdale, C. J., & Smith, H. E. 1999, ApJ, 511, 178
Herrnstein, J. R. *et al.* . 1999, Nature, 400, 539
Lonsdale, C. J., Lonsdale, C. J., Diamond, P. J., & Smith, H. E. 1998, ApJ, 493, L13
Pihlström, Y. M., Conway, J. E., Booth, R. S., Diamond, P. J., & Polatidis, A. G. 2001, A&A, 377, 413
Taylor, J. H. & Cordes, J. M. 1993, ApJ, 411, 674
Walker, M. A. 1998, MNRAS, 294, 307

TABLE 2
OH LINE MODULATION, SCINTILLATION PREDICTIONS, AND ACCELERATION IN IRAS 21272+2514

Feature	$\langle f_\nu \rangle_t$[a] (mJy)	$\langle F \rangle_t$[b] (mJy MHz)	m_s (%)	Scintillation Predictions θ_s (mas)	τ_s (days)	D_s (pc)	$\langle \nu_{pk} \rangle_t$ (MHz)	a (km s^{-1} yr^{-1})
(1)	(2)	(3)	(4)	(5)	(6)	(7)	(8)	(9)
1	12.3	7.06	10.4 ± 1.6	< 0.76	10–22	< 1.9	1449.099 ± 0.031	3.4 ± 3.6 (5)
2	12.2	9.27	14.4 ± 1.6	< 0.58	10–17	< 1.4	1449.901 ± 0.029	-5.5 ± 2.4 (4)
3	8.8	4.13	4.0 ± 1.9	> 1.74	> 51	> 4.2	1448.523 ± 0.013	-2.6 ± 0.8 (5)
4	5.3	4.93	4.4 ± 1.9	> 1.60	> 47	> 3.9	1451.560 ± 0.017	-2.6 ± 1.6 (5)
5	1.7	1.59	8.0 ± 4.3	> 0.96	> 28	> 2.3	···	···

[a]Uncertainties in the peak flux densities are ±0.2 mJy, excluding possible systematic calibration errors.

[b]Uncertainties in the integrated line flux densities are ±0.03 mJy MHz, excluding possible systematic calibration errors.